AIAA JOURNAL
Vol. 39, No. 2, February 2001

Experimental Study of Shear-Layer/Acoustics Coupling in Mach 5 Cavity Flow

Ö. H. Ünalmis,* N. T. Clemens,† and D. S. Dolling‡
University of Texas at Austin, Austin, Texas 78712

Simultaneous planar laser imaging and fluctuating-pressure measurements were made in a high-Reynolds-number, Mach 5 cavity flow, with cavity length-to-depth ratios of 3, 4, 5, 6, and 7. Instantaneous planar laser scattering images show no evidence for coherent structures that are induced by the cavity acoustics. Furthermore, both the pressure measurements and imaging suggest that the rear-wall shock is caused by the impingement of shear-layer turbulent structures. Analysis of the fluctuating-pressure data suggests that the shock frequencies and the duration of the impingement shock are not sensitive to cavity length-to-depth ratio. Ensemble-average velocity profiles in the shear layer, conditioned on the front-wall pressure, suggest that the deflection of the shear layer is not measurably correlated with the cavity oscillation cycle. In addition, spectral analysis of the fluctuating pressures shows that the cavity oscillation frequencies are accurately predicted using simple closed-box acoustic theory. These results suggest that the present cavity flow exhibits substantially less coupling between the cavity pressure fluctuations and the shear-layer fluid dynamics as compared to similar flows at lower Mach numbers.

Nomenclature

a	=	sonic speed
C_f	=	skin-friction coefficient
F_s	=	sampling frequency
FW1	=	uppermost front-wall pressure transducer
f	=	frequency
H	=	cavity depth, and boundary-layer shape factor
k_c	=	ratio of vortex convection speed to freestream flow speed, U_c/U_∞
L	=	cavity length
M	=	Mach number
n	=	mode number
P	=	instantaneous pressure
Re	=	Reynolds number
RW1	=	deepest rear-wall pressure transducer
RW7	=	uppermost rear-wall pressure transducer
R_{12}	=	cross-correlation coefficient between upstream and downstream pressure signals
r	=	recovery factor
SPL	=	sound pressure level, $20 \log_{10}\{\sqrt{[\Delta f \phi(f)]}/0.00002\}$
T, T_s	=	temperature and time delay between two consecutive shocks
t, t_d	=	time and shock duration
U	=	local mean velocity
U_c	=	convection velocity
W	=	cavity width
X	=	streamwise coordinate
Y	=	vertical coordinate
α	=	phase constant between the vortex shedding and the acoustic wave response in the cavity
γ	=	specific heat ratio of the gas
δ_0	=	boundary-layer velocity thickness, $0.99U_\infty$
δ^*	=	boundary-layer displacement thickness
θ	=	boundary-layer momentum thickness
Π	=	wake strength
ρ	=	density
σ	=	standard deviation of the fluctuating-pressure signal
$\Phi(f)$	=	power spectrum

Subscripts

L	=	longitudinal
m	=	mean condition
th	=	threshold condition
θ	=	based on momentum thickness
∞	=	freestream condition
0	=	stagnation condition

Received 2 September 1999; revision received 3 July 2000; accepted for publication 7 July 2000.

*Research Associate, Center for Aeromechanics Research, Department of Aerospace Engineering and Engineering Mechanics. Member AIAA.

†Associate Professor, Center for Aeromechanics Research, Department of Aerospace Engineering and Engineering Mechanics. Senior Member AIAA.

‡Professor, Center for Aeromechanics Research, Department of Aerospace Engineering and Engineering Mechanics. Fellow AIAA.

Introduction

INTERNAL carriage of stores offers many benefits for transonic and supersonic military aircraft, including elimination of store aerodynamic heating, reduction of aircraft drag and radar signature, greater maneuverability, and enlarged flight envelope. However, flight tests and extensive experimental and computational studies over the past 40 years have shown that airflow past cavities, such as aircraft weapons bays, can induce intense, self-sustaining pressure oscillations in and around the cavity. Dynamic loads on the rear bulkhead and at the junction of the rear bulkhead and cavity floor can be particularly severe. Spectra of the pressure fluctuations reveal discrete resonances whose frequency and amplitude depend on the cavity geometry and external flow conditions, as well as a broadband component typical of the turbulent shear layer. These pressure fluctuations can excite vibration of the local bay structure or store components resulting in damage to the stores and/or instrumentation failure, structural fatigue, and increased aerodynamic loading on the aircraft. They can also have detrimental effects on the stable release of weapons and their subsequent trajectories.

A review of much of the early work in subsonic and supersonic flows was compiled by Charwat et al.[1] in 1961. In the late 1970s Rockwell and Naudascher[2] published a detailed review of 78 studies, in which they developed a general framework for describing the various flow types. A brief, more recent review, including work of the 1980s and early 1990s with a focus on the control of cavity flow oscillations, can be found in Ref. 3. One observation from this large body of work is that there are relatively little published data at high supersonic or moderately hypersonic speeds. Accordingly, it is not clear if physical models based on subsonic and transonic external flows, which involve a strong coupling between the cavity acoustics and shear-layer dynamics, are also applicable to higher-Mach-number flows.

Based on his shadowgraph studies of subsonic and transonic shallow ($L/H > 1$) cavities, Rossiter proposed an empirical formula for predicting the frequencies of the oscillation modes.[4] Although the

mode frequencies can be predicted quite well by improved versions of his formula, such as that proposed by Heller and Bliss,[5] no analytic method is widely available for predicting the fluctuation amplitudes. In 1991, Bauer and Dix[6] did present a relatively simple analytic technique, which uses the modified Rossiter[4] equation for predicting frequencies, to predict amplitudes by modeling the shear layer as "a single-stream turbulent mixing zone, with the maximum wall pressure defined as a function of the rms kinetic energy in the turbulent mixing zone along the dividing streamline." An empirical damping term was used in the frequency response equation for the cavity. Although results were quite good, Bauer and Dix[6] noted that "correlation with spectral data was weak in the supersonic regime," raising questions about the appropriate flow physics at higher Mach numbers.

Sinha et al.[7] have recently examined the pros and cons of Reynolds-averaged Navier–Stokes (RANS) modeling and large eddy simulation of open cavity flows. An open cavity flow is one in which the shear layer bridges the cavity and reattaches on the downstream wall of the cavity.[1] Sinha et al.[7] concluded that 1) RANS-based two-equation techniques were too dissipative and suppressed the acoustic field, whereas RANS-based algebraic modeling resulted in severe underprediction of the dynamic loads, and 2) very large eddy simulation (VLES) provided a "good representation of the interactions between narrow-band acoustic tones and broad-band vortical structures"[7] and had the potential to provide a credible prediction of both static and dynamic loads. As VLES solutions at higher Mach numbers become more commonplace, the question of appropriate measurements for validation will become more critical.

Understanding the structure of cavity flow at higher Mach numbers is important not only for validation of simulations but for practical applications. Currently there is interest in opening weapons bays and releasing weapons at supersonic speeds because this eliminates the need for the aircraft to decelerate to subsonic speed, which in turn reduces time over target and enhances survivability. In the longer term, the development of techniques for suppressing the large-amplitude pressure oscillations will hinge on a clear understanding of the flow structure. In the current study, a combination of planar laser scattering (PLS), particle image velocimetry (PIV), and fast-response surface-pressure transducers have been used to gain a better understanding of the coupling between the cavity acoustics and the shear-layer dynamics. The experiments were conducted at Mach 5 in a high-Reynolds-number, turbulent, open cavity. The cavity length-to-depth ratio L/H was varied from 6 to 7. When necessary, data acquired for L/H of 3, 4, and 5 in the same facility were included in the analysis. The boundary-layer thickness-to-depth ratio of 0.76 was high compared to a typical weapons bay application, and, thus, this study was not an attempt to provide data for engineering design. It was intended that the experiments would prove helpful in shedding light on the underlying flow physics and aid in assessing the accuracy of computational models of cavity flow.

Experimental Program

Wind-Tunnel and Flow Conditions

All of the experiments were conducted in the Mach 5 blowdown wind tunnel at the University of Texas at Austin. The constant-area test section is 6 in. (15.2 cm) wide ×7 in. (17.8 cm) high and has a length of 30 in. (76.2 cm). Removable side doors allow access to the instrumented floor section. A total of about 140 ft^3 (4 m^3) of compressed air is provided by a Worthington HB4 four-stage compressor and stored in external tanks at a pressure of about 2500 psia (17.24 MPa). Two banks of nichrome wire resistive heaters (420 kW each) located upstream of the stagnation chamber heat the incoming air to the desired stagnation temperature, which is measured by a Type J thermocouple. The stagnation chamber pressure and temperature for the present experiments were 333 psia (2.29 MPa) ±1% and 635°R (353 K) ±1%, which, for a test section Mach number of 4.95, result in a freestream Reynolds number of 15.24×10^6/ft (50×10^6/m). The freestream velocity is 2509 ft/s (765 m/s). For these stagnation conditions, stable run times of up to 1 min can be obtained.

The incoming turbulent boundary layer undergoes natural transition and develops under approximately adiabatic wall temperature conditions. Shown in Table 1 are the values of basic parameters δ_0, δ^*, H, Π, Reynolds number Re_θ, and C_f of the undisturbed turbulent boundary layer on tunnel centerline at approximately the location of the cavity model in the test section.

Table 1 Incoming boundary-layer parameters in the Mach 5 test section

Parameter	Value
δ_0, in. (cm)	0.76 (1.93)
δ^*, in. (cm)	0.36 (0.91)
$H \equiv \delta^*/\theta$	12
Π	0.44
Re_θ	3.8×10^4
$C_f (\times 10^4)$	7.6

Instrumentation and Data Acquisition

Fluctuating-pressure measurements were made using Kulite Semiconductor Products, Inc., Model XCQ-062-15A and XCQ-062-50A transducers. These transducers have a nominal outer diameter of 0.0625 in. (0.159 cm) and a pressure-sensitive diaphragm of 0.028-in. (0.071-cm) diameter. Perforated screens above the diaphragm protect the transducer from being damaged by dust particles in the flow, but limit the frequency response of both models to about 50 kHz. For comparison, the characteristic frequency of the larger shear-layer structures is expected to be of order U_∞/S, where S is the structure spacing (1–2 δ_0) and corresponds to a frequency of 20–40 kHz. The transducers were flush mounted on two blocks [3 in. (7.62 cm) wide by 1 in. (2.54 cm) high by 1 in. long] that serve as the front and rear walls of the cavity.

Output from the Kulite® pressure transducers was amplified by either Dynamics (Model 7525), Vishay Measurements Group (Model 2311), or PARC (Model 113) amplifiers. The amplified signals were then filtered using Ithaco (Models 4113 or 4213) analog filters. A sampling rate of 200 kHz was used in most of the experiments and the filter cutoff was set at 40 kHz. The peak signal-to-noise ratio was about 200.

Pressure data were acquired using two LeCroy A/D converters with 12-bit resolution (Model 6810 waveform recorders). Each A/D converter has 4 MB of memory and can sample one channel of data at rates up to 5 MHz, or four channels of data simultaneously at rates up to 1 MHz per channel. The two A/Ds can acquire data from eight channels simultaneously when triggered using the same clock. For the current work, depending on the interest and L/H of the cavity, two, four, six, or eight channels were used. The frame grabber and the laser firing (Q switch) synchronization signals were also recorded to determine the image acquisition time precisely. For the fluctuating-pressure measurements only, 524,288 data points were acquired per channel with a sampling frequency of 200 kHz. For simultaneous fluctuating-pressure and PLS (or PIV) measurements, 4096 data points per channel were acquired for each PLS (or PIV) image. For simultaneous measurements the A/D converters were pre-triggered: Once the laser fired, it triggered the A/D, and the A/D assigned the triggering time as the center of the total 4096 data points for each channel, thus acquiring 2048 data points before and after the triggering time.

Cavity Models

The results of the current study are from experiments using a rectangular cavity model, for which L/H can be varied from 6 to 8, as well as from analysis of data obtained from previous work[3,8,9] using a cavity model with L/H ratios of 3, 4, and 5.

Figure 1 shows a schematic diagram of the tunnel floor, which has a 3 in. (7.6 cm) wide × 8 in. (20.3 cm) long cutout that forms the front, rear, and side walls of the cavity. The nominal depth of the cavity is 1 in. (2.54 cm). A bottom plate is then used to form the cavity floor. On the centerline of the cavity floor there is a slot that is 0.25 in. (0.64 cm) wide and 6.9 in. (17.53 cm) long. This slot accepts a fused silica window that is antireflection coated on both sides. The fused silica allows the laser sheet to pass through and thereby reduces the background scattering from the floor and side walls of the cavity in the PLS experiments. The cavity floor plate

and the fused silica window are both 0.5 in. (1.27 cm) thick. This arrangement substantially reduced the elastic scattering from the floor of the cavity.

The pressure transducers were flush mounted in two 1-in. (2.54-cm) blocks and placed at the upstream and downstream ends of the cavity (Fig. 1). The rear-wall transducers were used to monitor the shear-layer impingement (and subsequent bow-shock generation) at the top of the rear wall, whereas the front-wall transducers were used to calculate space–time correlations between the front- and rear-wall pressure signals. In particular, they were used to examine the propagation of the acoustic wave, which is linked to the shear-layer impingement. With the rear block in place, a maximum nominal L/H of 7 can be obtained. With this L/H ratio, the cavity flow is an open type, that is, the separated shear layer bridges the cavity and reattaches onto the downstream face of the cavity.

PLS

The PLS imaging technique relies on laser light scattering from a fine ethanol fog and has been previously applied in high-Mach-number cavity flows.[10–12] In the current work, the ethanol was directly injected into the plenum section using three fine spray atomizing nozzles (Spraying Systems LN30). The ethanol was supplied using a stainless steel reservoir of capacity 2 ft^3 (0.057 m^3), which was pressurized to 600–750 psia (4.1–5.2 MPa). The flow then passed through a fine mesh screen before entering the plenum.

Optical access through the side of the test section was provided by a fused silica window of dimensions 6 in. (15.2 cm) long × 2 in. (5.1 cm) high × 0.75 in. (1.9 cm) thick. A narrow acrylic window, 9 in. (22.9 cm) long × 0.5 in. (1.27 cm) wide × 0.75 in. (1.9 cm) thick, provided access for the laser sheet through the top of the test section. Side-view images were obtained by passing the laser sheet vertically through the top window and with the camera oriented at 90 deg to the sheet.

A schematic diagram of the PLS imaging setup is shown in Fig. 2. Either an Nd:YAG Spectra-Physics GCR-150 (single-pulse capable) or a PIV-400 (double-pulse capable) laser was used as the light source of the system. The laser was frequency doubled to 532 nm and operated at 10 Hz. For the PLS experiments, the Nd:YAG laser provided energy of about 35–55 mJ per pulse. The laser beam was formed into a sheet approximately 5.5 in. (14 cm) wide and 0.01 in. (254 μm) thick using a spherical and a cylindrical lens. The scattering was imaged with a charge-coupled device (CCD) video camera (Cohu 4990), which was operated in a frame-straddling mode for the double-pulse imaging experiments. The images were digitized using a frame grabber (DataTranslation DT2851) installed in a 486 IBM-compatible personal computer with sufficient memory to store 90 images of resolution 240 × 512. Image processing was done using the Khoros 1.0 image-processing package.

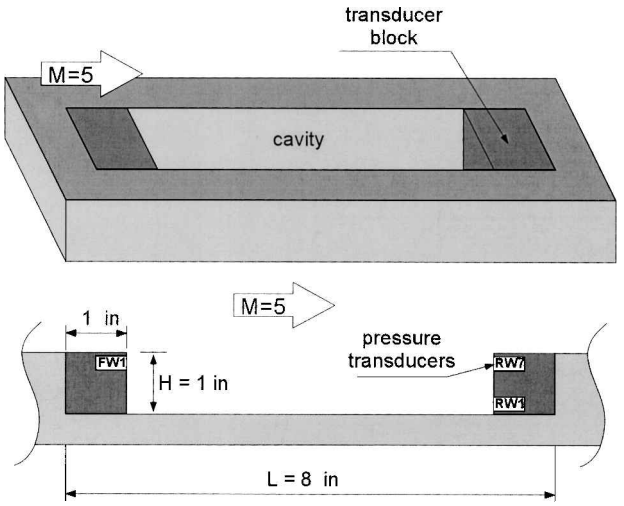

Fig. 1 Cavity geometry and transducer blocks.

PIV

In the current study a dual-cavity Nd:YAG laser (Spectra-Physics PIV-400) was used for the PIV image acquisition (Fig. 2). The laser was operated at 10 Hz and with an energy per pulse of about 70 mJ. Particle images were captured with a 1000 × 1000-pixel frame-straddling CCD camera (Kodak ES 1.0), with a typical pulse delay time Δt of 1.4 μs. With this Δt, the maximum particle displacement was less then 0.04 in. (1 mm). The use of frame straddling (i.e., the recording of the particle images on two separate frames) has the advantage that it eliminates the directional ambiguity problem that is associated with the double-exposure approach.

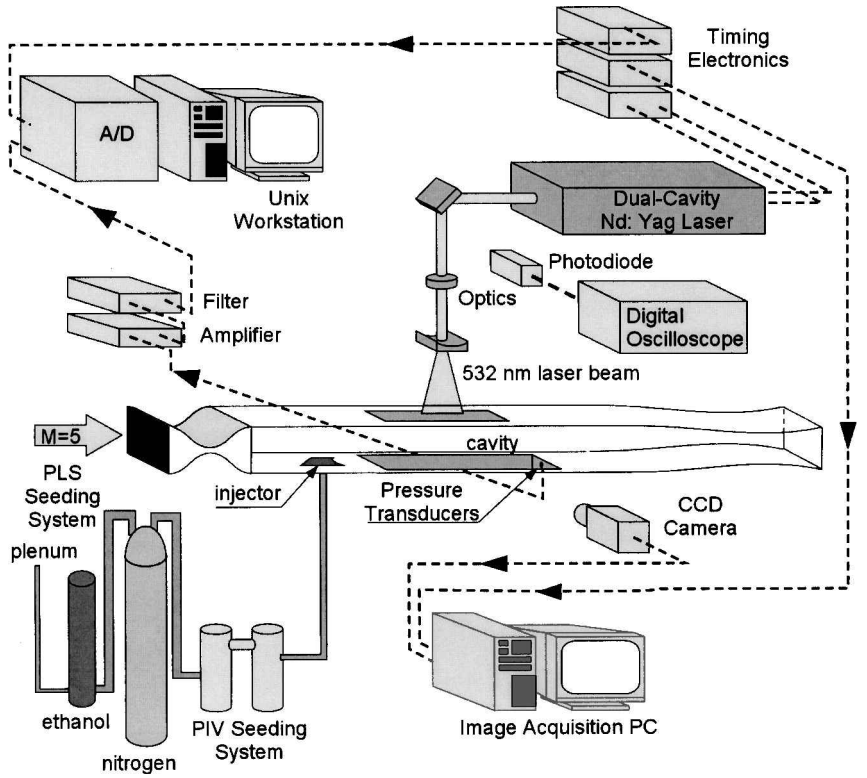

Fig. 2 Experimental setup for PLS and PIV experiments.

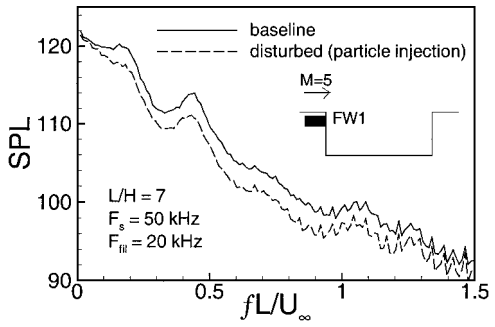

Fig. 3 Effect of injector on the SPL at the front wall.

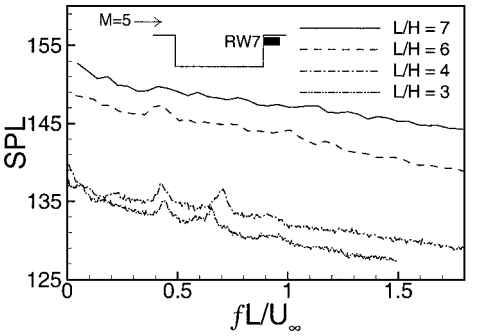

Fig. 4 SPL for the uppermost rear-wall transducer (RW7).

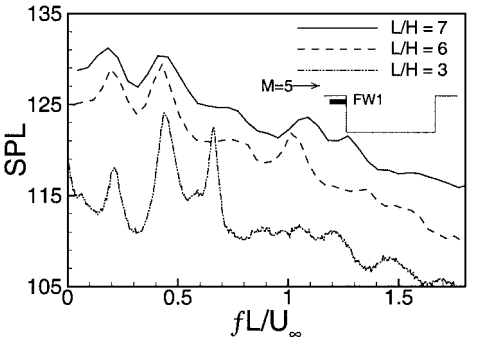

Fig. 5 SPL for the uppermost front-wall transducer (FW1).

The synchronization of the system was achieved using two delay/pulse generators (Stanford Research Systems DG535). The first DG535 generated a 10-Hz signal to drive the laser flashlamps and Q switches. The second DG535 was triggered externally by the first DG535 and provided the triggering signals for the CCD camera and the A/D for the acquisition of fluctuating-pressure signals. The energy levels of the two pulses were balanced using a fast photodiode that was connected to a digital oscilloscope (Tektronix TDS 520C). The images were processed on a personal computer Linux workstation through a custom program developed in-house.[13,14]

The particles used were aluminum oxide (Al_2O_3) with a manufacturer's specification of 0.1 μm diameter and were delivered using a two-stage fluidized bed seeder. During a tunnel run, when the stagnation pressure reached a steady value, a valve that connects a nitrogen source to the fluidized bed was opened to drive the particles into the flow through a streamlined injector. The injector was installed on the floor just downstream of the nozzle, 20 in. (0.5 m) upstream of the cavity front wall. The injector was 0.6 in. (1.52 cm) high $\times$0.55 in. (1.4 cm) wide $\times$4.3 in. (10.9 cm) long in the streamwise direction. The leading- and trailing-edge surfaces were swept toward the center of the injector, yielding an appearance akin to a tapered diamond shape. To assess the potential interference on the cavity flow with the injector upstream, fluctuating-pressure measurements were made with and without the injector in place. Figure 3 shows the sound pressure levels (SPL) of the signals recorded by the front-wall pressure transducer for two different cases: 1) baseline case, no injector and 2) disturbed case, injector in place with particle injection. The sampling frequency was 50 kHz, and the signals were filtered at 20 kHz. Figure 3 shows that the mode frequencies are largely unaffected, but the amplitude of the pressure oscillations is decreased with the injector in place and operating. Overall, the rms of the fluctuations for injector with particles on is reduced by 15%, compared to the baseline case. Only the first two modes are evident and occur at Strouhal numbers of 0.19 and 0.44, respectively. Note that the sound pressure spectra are more broadband compared to those found in low-Mach-number cavity flows[2,15,16] where the peaks in the power spectra of the pressure signals have much higher amplitudes.

Results

Oscillatory Mode Frequencies

Power spectra in the form of SPL vs Strouhal number for the uppermost transducer (RW7) that is located on the rear wall 0.125 in. (0.32 cm) below the cavity lip are plotted in Fig. 4 for four L/H ratios. (The transducer labels are the same as used in the related work of Perng and Dolling.[9]) The cases $L/H = 3$ and 4 are from Ref. 9. Comparison of the power spectra shows that as L/H increases, the overall SPL increases for all frequencies (for comparison, for a Strouhal number of 0.5, the SPL for $L/H = 4$, 6, and 7 are larger by about 2, 9, and 12%, respectively, compared to that for $L/H = 3$) and that the spectra become more broadband (or the spectral peaks become less distinct). This result is expected because the shear-layer impingement occurs closer to the cavity floor on the rear wall with increasing L/H and consequently higher-energy fluid enters the cavity, thus increasing the local pressure fluctuations.

The power spectra for the uppermost transducer on the front wall (FW1), which is 0.125 in. (0.32 cm) below the cavity lip, are plotted in Fig. 5 for $L/H = 3$, 6, and 7. The $L/H = 3$ case is from Ref. 8. A comparison of Figs. 4 and 5 shows that the mode frequencies are more evident on the front wall than on the rear wall. This is probably because the noise level near the rear wall is increased by the impinging turbulent shear layer and the intermittent impingement shock at the top edge of the rear wall. Examination of the front-wall pressure spectra shows that the first two oscillatory modes occur at approximately the same Strouhal number for all cases, whereas this is not true for the third and fourth modes. Figure 5 also shows that for the first mode, the power level increases as L/H increases, whereas for the second mode the peak for the shorter cavity is sharper. For cavities with $L/H = 6$ and 7, the third mode is less prominent, whereas it is very distinct in the case of $L/H = 3$.

The experimental mode frequencies are compared with values calculated using Rossiter's[4] modified formulas as well as with classical closed-box acoustic modes of the cavity and are given in Table 2. The modified formula[5] is given by

$$\frac{fL}{U_\infty} = \frac{n - \alpha}{\left[M_\infty \Big/ \sqrt{1 + (r/2)(\gamma - 1)M_\infty^2}\right] + (1/k_c)} \qquad n = 1, 2, 3, \ldots \quad (1)$$

where n is the mode number, α is the phase constant between the vortex shedding and the acoustic wave response in the cavity, and k_c is the ratio of the average vortex convection speed to the freestream flow speed. Appropriate values of the empirical parameters α and k_c and their dependence on flow conditions and L/H is an unresolved issue and is discussed in some detail by Bauer and Dix[6] and Perng.[3] Bauer and Dix[6] fitted Rossiter's[4] values of α (obtained in the Mach number range of 0.4–1.2) to linear and second-order curves in terms of L/H, which, for $L/H = 6$ (and 7), give values for α of 0.38 (and 0.44) and 0.40 (and 0.46). Bauer and Dix[6] also report that a value of 0.57 has been quite widely accepted for k_c, although they note that East[17] had suggested it could be as high as 0.65. Bauer and Dix[6] also point out that the value of 0.57 is, strictly speaking, restricted to a thin initial boundary layer, which is not the case for the current experiment. They attempted to include the effect of an initial boundary layer by assuming that the vortices moved at the velocity of the dividing streamline. This approach resulted in a semi-empirical expression for k_c whose leading term is the theoretical incompressible value of 0.6163, which is then modified for compressibility by a term involving Mach number and a turbulent

Table 2 Experimental and calculated mode frequencies for $M = 4.95$

			Eq. (1), $r = 1$				Eq. (1), $r = 0.89$ (Heller and Bliss[5])	
			Rossiter[4]		Bauer and Dix[6]			
L/H	Mode n	Strouhal number (measured)	Eq. (2), $r = 1$	$k_c = 0.57$, $\alpha = 0.25$	$k_c = 0.9$, $\alpha = 0.25$	$k_c = 0.7044$, α (linear)	$k_c = 0.9$, α (linear)	$k_c = 0.47$, $\alpha = 0$	$k_c = 0.9$, $\alpha = 0$
						$\alpha = 0.21$	$\alpha = 0.21$		
3	1	0.21	0.24	0.20	0.24	0.23	0.25	0.23	0.31
	2	0.43	0.49	0.46	0.56	0.52	0.57	0.47	0.62
	3	0.66	0.73	0.73	0.87	0.81	0.89	0.70	0.93
	4	0.88	0.98	0.99	1.19	1.10	1.20	0.94	1.23
						$\alpha = 0.27$	$\alpha = 0.27$		
4	1	0.22	0.24	0.20	0.24	0.21	0.23	0.23	0.31
	2	0.42	0.49	0.46	0.56	0.52	0.55	0.47	0.62
	3	0.71	0.73	0.73	0.87	0.81	0.87	0.70	0.93
	4	0.95	0.98	0.99	1.19	1.10	1.18	0.94	1.23
						$\alpha = 0.32$	$\alpha = 0.32$		
5	1	0.23	0.24	0.20	0.24	0.20	0.22	0.23	0.31
	2	0.42	0.49	0.46	0.56	0.49	0.53	0.47	0.62
	3	0.75	0.73	0.73	0.87	0.78	0.85	0.70	0.93
	4	1.05	0.98	0.99	1.19	1.06	1.17	0.94	1.23
						$\alpha = 0.38$	$\alpha = 0.38$		
6	1	0.17 – 0.23	0.24	0.20	0.24	0.18	0.20	0.23	0.31
	2	0.41 – 0.45	0.49	0.46	0.56	0.47	0.51	0.47	0.62
	3	0.72 – 0.76	0.73	0.73	0.87	0.76	0.83	0.70	0.93
	4	0.98 – 1.04	0.98	0.99	1.19	1.05	1.15	0.94	1.23
						$\alpha = 0.44$	$\alpha = 0.44$		
7	1	0.17 – 0.23	0.24	0.20	0.24	0.16	0.18	0.23	0.31
	2	0.41 – 0.45	0.49	0.46	0.56	0.45	0.50	0.47	0.62
	3	0.70 – 0.75	0.73	0.73	0.87	0.74	0.81	0.70	0.93
	4	1.04 – 1.10	0.98	0.99	1.19	1.03	1.13	0.94	1.23

mixing position parameter. At $M = 4.95$, this formula gives a mathematical upper bound for k_c ($k_c \leq 0.7044$). Perng[3] reviewed the work of Zhang and Edwards,[18] Maciulaitis,[19] and Rossiter,[4] spanning the Mach number range 0.4–2.5, and noted that the suggested values of k_c ranged up to 0.75. Experimentally, the current results suggest that k_c could be even higher. Based on inferring structure convection velocities from double-pulse images, it would appear that values of k_c could be as high as 0.9. Accordingly, it is not entirely clear what values of k_c and α should be used to calculate the mode frequencies. Table 2 shows predictions for several different combinations.

The closed-box acoustic modes[20] are modeled as the longitudinal modes in a box of length L filled with air with stagnation speed of sound a_0. The resonance frequencies are then given by $f_L = (a_0/2L)n$, with Strouhal number,

$$\frac{f_L L}{U_\infty} = \frac{\left[1 + (r/2)(\gamma - 1)M_\infty^2\right]^{\frac{1}{2}}}{2M_\infty} n, \qquad n = 1, 2, 3, \ldots \quad (2)$$

Before discussing the comparisons of the predictions and measurements, the following should be noted. The issue of the presence of shedding vortices has been a topic of some controversy: More than 20 years ago, Tam and Block[21] raised questions about Rossiter's[4] model, which, to the present authors' knowledge, have still not been answered satisfactorily and which are being addressed in the current work. Tam and Block[21] noted that "a good deal of significance is attached to the highly localized vortices" yet schlieren photographs taken by Krishnamurty[22] and by Heller et al.[23] "did not indicate the presence of these vortices during cavity oscillations."[21] Tam and Block[21] suggested that "vortex shedding is probably not important over the entire Mach number range as far as cavity oscillations are concerned." Support for that view comes from the current experiments as presented in the following sections.

The experimental values of the mode frequencies, the closed-box acoustic mode frequencies, and the mode frequencies computed from Rossiter's[4] modified formula with different sets of k_c and α are plotted in Fig. 6 in the form of Strouhal number vs mode number n for $L/H = 7$. Examination of Fig. 6 (and Table 2) shows that the simple closed-box acoustic modes are often in better or equal agreement with the measured values compared to those predicted by the models. When k_c is assumed to be 0.9, a value inferred from double-pulse side-view PLS images in the current study, all of the models predict the mode frequencies rather poorly.

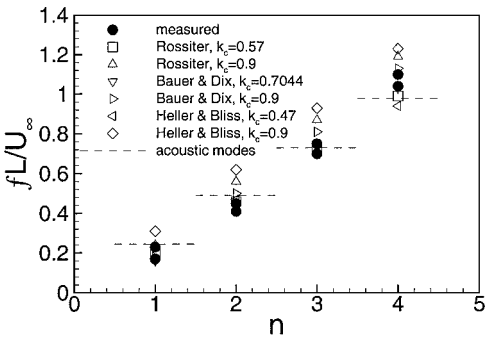

Fig. 6 Comparison of Strouhal numbers based on the measured Mach 5 cavity resonance frequencies, acoustic modes, and some common models for different mode numbers ($L/H = 7$).

To determine if closed-box acoustics successfully predicts oscillation frequencies for different length cavities, Strouhal numbers based on the measured Mach 5 cavity resonance frequencies and corresponding acoustic modes from Table 2 are presented in Fig. 7 as a function of L/H. Note that the experimental data agree well with the acoustic modes regardless of the value of L/H.

The success of the closed-box acoustics in predicting the measured data is consistent with the findings of Heller et al.[23] They found that as the Mach number increases the mode frequencies approach the acoustic modes of a cavity. Based on this result, they suggested that the interface between outer and inner flows creates a larger acoustic impedance as Mach number increases. As a result, "the closed-box frequencies are then approached."[23]

To investigate this effect further, the subsonic and supersonic data of Clark et al.,[24] Bauer and Dix,[6] and the present study are shown plotted together in Fig. 8. Figure 8 shows, as suggested by Heller et al.,[23] that at low Mach numbers acoustic theory does not correctly predict the resonance frequencies; hence the need for Rossiter's[4] formula. In contrast, as the Mach number increases, the measured

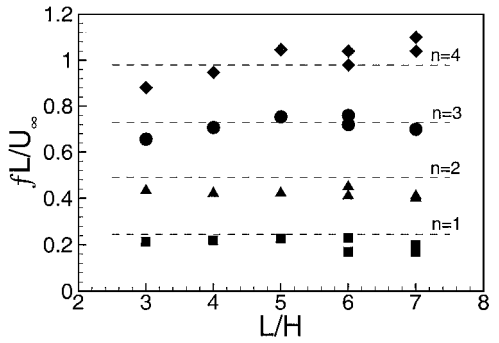

Fig. 7 Strouhal numbers based on the measured Mach 5 cavity resonance frequencies and corresponding acoustic modes (– – –) as a function of *L/H*.

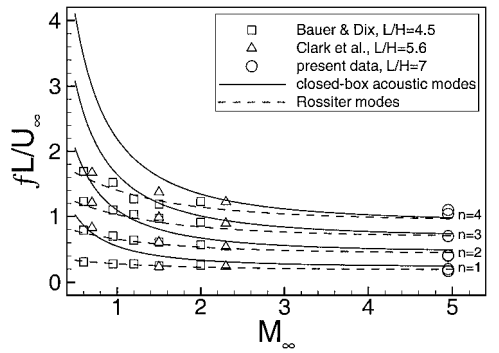

Fig. 8 Variation of Strouhal numbers (based on cavity resonance frequencies) with Mach number and comparison with closed-box acoustic and Rossiter modes.

resonance frequencies approach the acoustic modes. Because the purely acoustic model includes no information about the shear-layer dynamics, this seems to suggest that the coupling between the shear layer and the cavity pressure oscillations in low-Mach-number flows may be less significant in high-Mach-number flows. This issue is investigated further in the following sections.

Characteristics of Shock Impingement Process

Earlier work[3,9] in the same facility with smaller L/H cavities has shown that the pressure signals on the rear wall exhibited high-magnitude spikes, which were attributed to the impingement shock events. These events create a large disturbance on the rear wall and, consequently, can be seen as the main source of the acoustic radiation. Because all of the existing models assume the periodic creation of acoustic radiation at the rear wall, the characteristics of these impingement shock events were investigated by means of the correlations of the signals from the rear and front wall.

The normalized cross correlation between the pressure signals on the front wall (FW1) and rear wall (RW7) are shown in Fig. 9a for $L/H = 3$ (from Ref. 8) and for $L/H = 6$. The time is normalized by L/U_∞. For $L/H = 3$, the peak value of the cross correlation is 0.16 and occurs at $tU_\infty/L = -2.138$. Assuming stagnant fluid in the cavity, the normalized time for an acoustic wave to travel from the rear wall to the front wall is 2.133, which suggests that the cause of the peak at $tU_\infty/L = -2.138$ is an acoustic wave. The results for $L/H = 6$ support this conclusion: The peak values of the cross correlation of the FW1 and RW7 signals occur at $tU_\infty/L = \pm 2.108$, within about 1% of the value for $L/H = 3$. Assuming that these peak values in the cross correlation are due to the propagation of an acoustic wave, the normalized period is $TU_\infty/L = 4.216$. The corresponding Strouhal number fL/U_∞ is then calculated as 0.237, which is close to the experimental value of the first mode given in Table 2.

The peak value of the cross correlation between signals at the top of the front wall (FW1) and bottom of the rear wall (RW1, 0.125 in. above the cavity floor) for $L/H = 3$ is 0.31 and occurs at $tU_\infty/L = -1.948$, whereas in the case of $L/H = 6$, these values

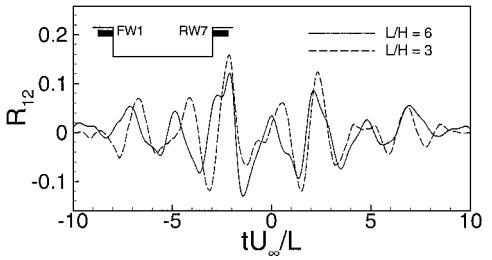

a) FW1 and RW7

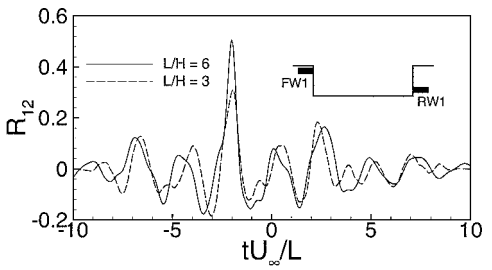

b) FW1 and RW1

Fig. 9 Normalized cross correlation of the fluctuating-pressure signals.

are 0.51 and −2.008, respectively (Fig. 9b). As expected, the cross-correlation curves are also very similar in this case, suggesting again that the same flow structure exists. The increase in the magnitude of the maximum cross-correlation coefficient with L/H is quite probably due to the increased amount of high-energy fluid inside the cavity: For a longer cavity, the impingement of the shear layer on the rear wall occurs closer to the cavity floor, and consequently, stronger pressure oscillations are generated.

Some important characteristics of the shock impingement process can be determined from these pressure measurements. Two characteristics that are important in understanding the cavity oscillation cycle are the duration of the shock t_d and the delay between two consecutive shock events T_s. To determine these parameters, the pressure signal from the uppermost transducer on the rear wall (RW7) was analyzed for three different L/H ratios (namely, 3, 6, and 7). The threshold value for detecting a shock event was chosen as $P_{\text{th}} = P_m + 2.5\sigma$, where P_m and σ are the mean and standard deviation of the pressure signal, respectively (Fig. 10a). The resulting signal then consists of a boxcar to represent the shock events (Fig. 10b). The duration of a shock event t_d was defined as $t_1 - t_2$, where t_2 refers to the time when the value of the pressure signal exceeds the threshold, and t_1 refers to the time when the value of the signal decreases below the threshold. The time between two consecutive shock events was defined as $t_2 - t_{2p}$, where t_{2p} refers to the starting point of the preceding shock event. Based on these definitions, the mean values of t_d and T_s can be found from

$$t_m = \overline{t_d} = \sum_{k=1}^{N} \frac{(t_1 - t_2)}{N}, \qquad T_m = \overline{T_s} = \sum_{k=1}^{N} \frac{(t_2 - t_{2p})}{N}$$

where N is the total number of shock events. Values of t_m for the three L/H ratios are plotted in Fig. 10c. Note that t_m does not seem to be sensitive to the cavity length-to-depth ratio and varies between 20 and 30 μs. Given $U_\infty = 765$ m/s and a large-scale structure length scale of order δ_0, this time scale is of the order that is required for the structure to convect past a given point. The mean time between two consecutive shocks T_m for the same cases is shown in Fig. 10d. Again, T_m does not seem to depend on the value of L/H, but ranges between 0.7 and 1 ms, corresponding to a frequency range of 1–1.4 kHz. If the shock events were coupled to the oscillation cycle, it would be expected that T_m would vary by a factor of 7/3 for L/H ranging from 3 to 7. The histogram for T_s is shown in Fig. 10e. The distribution of T_s is broad with a large tail, thus providing additional evidence that the shock event is not periodic.

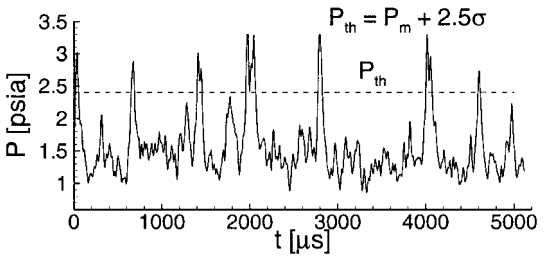

a) Pressure data at RW7 for $L/H = 6$ with example threshold (– – –)

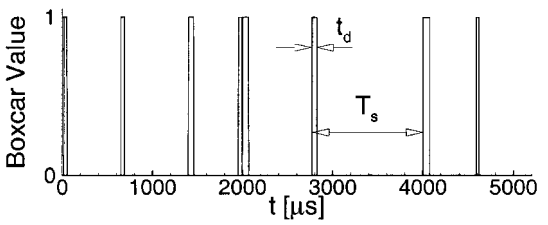

b) Corresponding boxcar signal

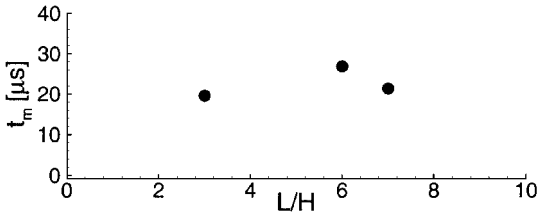

c) Average shock duration

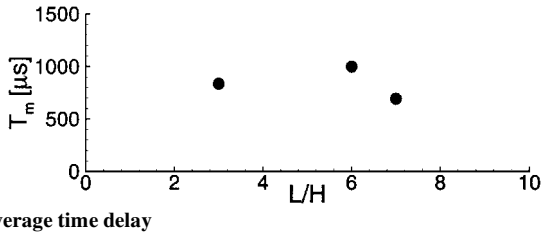

d) Average time delay

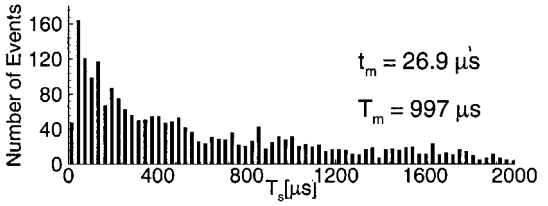

e) Time delay histogram for $L/H = 6$

Fig. 10 Shock impingement analysis.

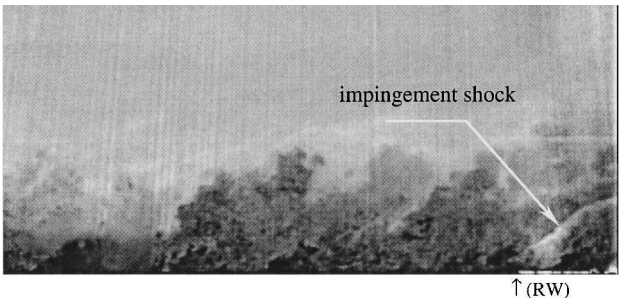

a) PLS image for the first laser pulse

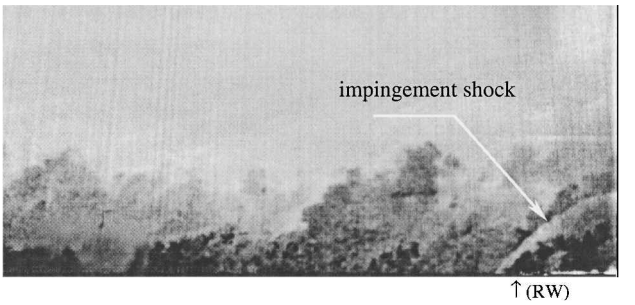

b) PLS image for the second laser pulse ($\Delta t = 30$ μs)

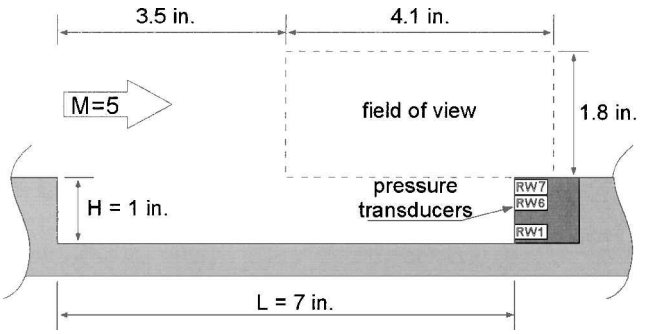

c) Field of view

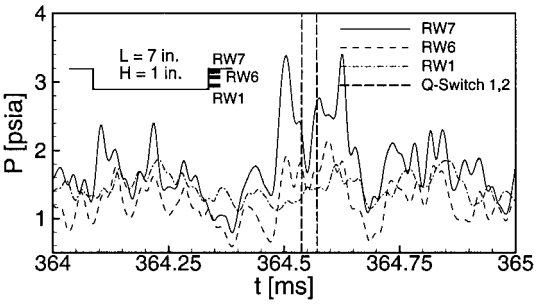

d) Corresponding fluctuating-pressure field (F_s = 500 kHz)

Fig. 11 Impingement shock at the rear wall of the cavity.

PLS Side-View Images

The planar imaging techniques were used to provide additional information on the role that the shear layer plays in the cavity oscillation process. In particular, imaging was used to address two specific issues. The first is whether the intermittent high pressures measured at the rear wall were being correctly interpreted as impingement shock events. This has a bearing on the conclusion drawn earlier that the shock events are not tightly coupled to the cavity oscillation cycle. The second issue addressed is whether there is any indication that the shear layer responds to forcing by the cavity pressure oscillations. Given the relatively low frequencies that characterize the strongest cavity oscillation modes, it is expected that such forcing would likely manifest itself as a large-scale flapping or deflection of the shear layer, rather than through the generation of identifiable vortex structures. These issues are discussed in the following two sections.

In the double-pulse image acquisition the time delay between the laser pulses was chosen to be 30 μs, during which time the shear layer is expected to move about 0.8 in. (2 cm) based on a convection velocity of 0.9 U_∞. Fluctuating-pressure data on the rear wall were also recorded simultaneously. Four sample image pairs are shown in Figs. 11–14 and correspond to four different distinct behaviors of the cavity flow. Figure 11 is an example of a case where the impingement shock at the rear wall exists for a relatively long time (160 μs). The field of view is about 4.1 in. (10.4 cm). The impingement shock can clearly be seen in both images owing to the density jump across the shock. This density jump results in higher scattering signals downstream of the shock. Because the temperature jump across the shock is large enough to evaporate the seed, the scattering signals do not remain high after the shock. The evaporation process is not instantaneous, however, as shown by the increase and then decrease in signal across the shock. Note that, in the first image, three large-scale shear-layer structures are seen that will soon reach the rear wall. In the second image, the second of the three structures reaches the rear wall. The pressure data (Fig. 11d) illustrate the process: After reaching a high value, probably due to earlier structures, the

a) PLS image for the first laser pulse

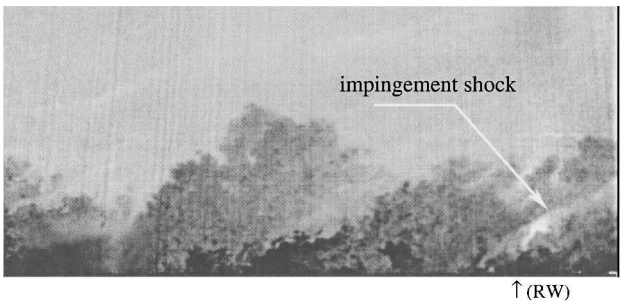

b) PLS image for the second laser pulse ($\Delta t = 30\ \mu s$)

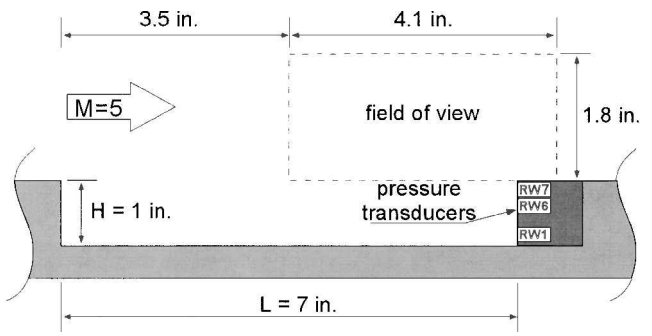

c) Field of view

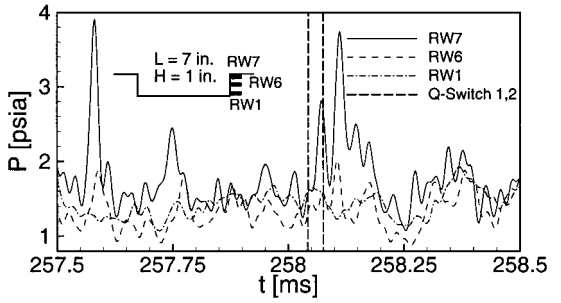

d) Corresponding fluctuating-pressure field ($F_s = 500$ kHz)

Fig. 12 Impingement shock develops between two laser pulses.

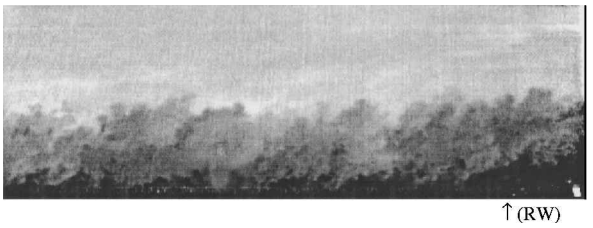

a) PLS image for the first laser pulse

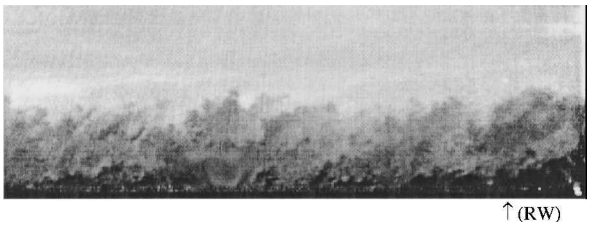

b) PLS images for the second laser pulse ($\Delta t = 30\ \mu s$)

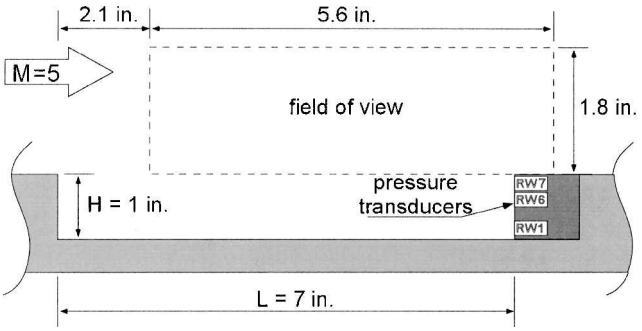

c) Field of view

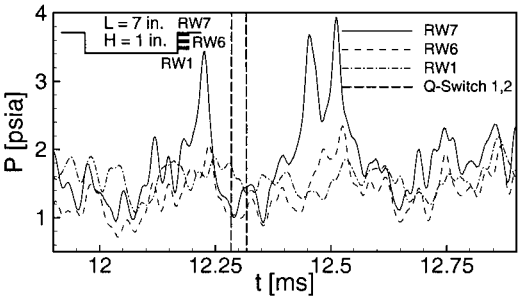

d) Corresponding fluctuating-pressure field ($F_s = 500$ kHz)

Fig. 13 Sample PLS images for low-pressure condition at the rear wall.

pressure is just about to decrease at the instant of the first image, yet it recovers and increases again at the instant of the second image as the first two of the three structures reach the rear wall. The last peak in the pressure data seems to be due to the impact of the last incoming structure.

A second example (Fig. 12) appears to show the development of an impingement shock. The field of view is the same as in Fig. 11. The image from the first pulse shows no indication of an impingement shock, which is confirmed by the low pressure at the time of the first laser pulse (Fig. 12d). At this instant, a large-scale shear-layer structure is about to pass by the rear-wall region. The pressure increases and a shock develops as the structure interacts with the rear wall (Figs. 12b and 12d). It would also be reasonable to assume that the large-scale structure in the middle of the second image is the cause of the subsequent pressure rise and possibly a stronger shock. These two examples show the critical role that the large-scale shear-layer structures play in the shock impingement process: The large-scale shear-layer structures not only change the duration of an existing shock at the rear wall but they alone may also be the cause for the formation of the shock. The third sample (Fig. 13) shows a PLS image pair where the shear layer seems very quiescent. The field of view is 5.6 in. (14.2 cm). The corresponding pressure signal shows that these quiescent instances are coincident with low-pressure values.

The existing models[4,5] of the cavity flow assume that one fundamental part of the oscillation cycle is mass ejection out of the cavity. In the current study, none of the acquired 180 image pairs provides any unambiguous evidence of mass ejection from the cavity. The only pair to provide a hint of such behavior is shown in Fig. 14. Unlike cases when the impingement shock is present, the dark region around the rear wall is larger. This dark region presumably marks the hot fluid inside the cavity where the fluid is too warm to sustain alcohol in the liquid or solid phase. The downstream half of the second image shows that there is a growth of this dark region with no indication in the first image that it is coming from upstream.

PLS images were also obtained near the front-wall region. In Fig. 15, the upstream region of the cavity is shown, where the field of view is 4.6 in. (11.7 cm) long and 1.8 in. (4.6 cm) high and

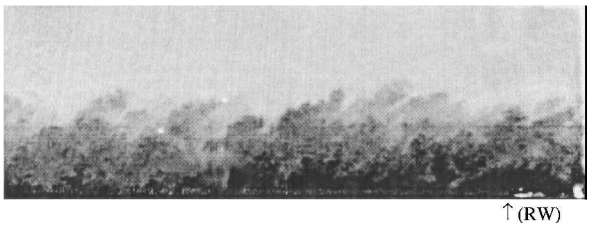

a) PLS image for the first laser pulse

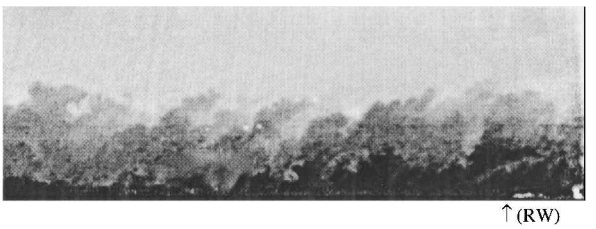

b) PLS image for the second laser pulse ($\Delta t = 30\ \mu s$)

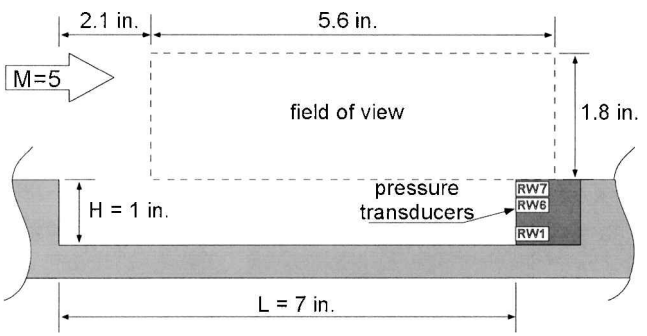

c) Field of view

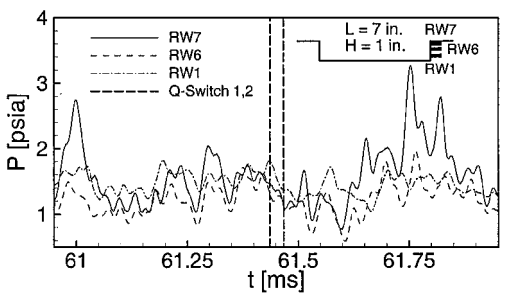

d) Corresponding fluctuating-pressure field (F_s = 500 kHz)

Fig. 14 Sample PLS images showing the ejection of fluid out of cavity.

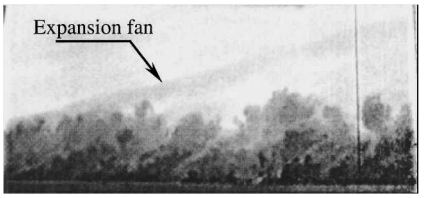

a) Instantaneous side-view PLS image

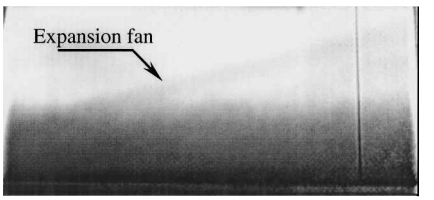

b) Ensemble-average side-view PLS image

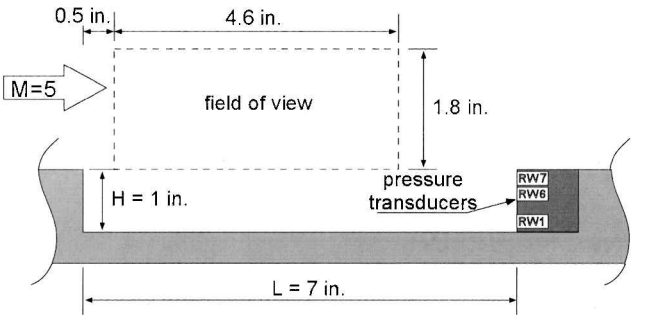

c) Field of view

Fig. 15 Side-view PLS images of the front-wall region.

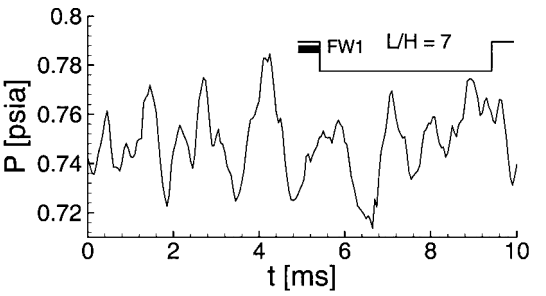

Fig. 16 Sample front-wall pressure signal.

extends from 0.5 in. (1.27 cm) to 5.1 in. (13 cm) downstream of the front wall (Fig. 15c). Figure 15a shows that the shear layer, although exhibiting a range of scales, does not appear to exhibit the coherent vortical structures that are observed at lower Mach numbers (such as in the work of Cattafesta et al.[16]). This observation applies to the vast majority of the hundreds of images that have been acquired. The lack of coherent structures is likely related to the high compressibility of the shear layer, as found by Murray and Elliott,[12] who observed large-scale coherent structures in the shear layer, above a Mach 1.8 cavity, but not for a Mach 3.5 cavity flow. Such reduced organization at high Mach numbers has also been observed in compressible planar mixing layers.[25]

Figure 15a also shows an expansion fan developing from the front edge of the cavity. Note that this expansion wave was not always present because it occurred in only about 60% of the images that were acquired randomly. Previous work[10] has shown that the deflection of the shear layer is usually masked by the structures in the outer part of the shear layer. Therefore, the deflection downward of the shear layer can be more likely detected implicitly, through the presence of an expansion wave. An ensemble-average image of the same field of view based on 90 random ensembles is shown in Fig. 15b, where the expansion fan is clearly visible. Based on the observation that an expansion wave appears and disappears around the front-wall region of the cavity, additional experiments were conducted to see whether a deflection, as determined by PIV, could be correlated with the fluctuating pressure in the cavity. This is discussed next.

Ensemble-Average Velocity Profiles

Although the rear-wall pressures are not highly periodic, Fig. 5 shows that the front-wall pressures are much more so (a sample time series is shown in Fig. 16). Furthermore, instantaneous side-view PLS images show that there are times when expansion waves appear around the front-wall region, and there are times when they disappear. To investigate whether the appearance of the expansion correlates with the quasi-periodic wall-pressure signal, additional experiments were made using PIV. The objective was to determine whether changes in the shear-layer velocity field, such as that induced by the flapping of the shear layer, could be detected at different phases of the oscillation cycle. This was done at four different stations in the shear layer.

The field of view for the fourth station is shown in Fig. 17. It is a 1.15-in. (2.92-cm) square window and extends from 4.95 in. (12.57 cm) to 6.1 in. (15.49 cm) downstream of the front wall. One pressure transducer was installed at the uppermost port of the front wall, and 4096 data points were recorded for each PIV image pair captured.

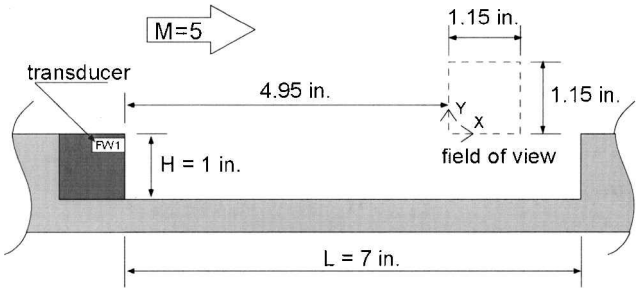

Fig. 17 Field of view for station 4.

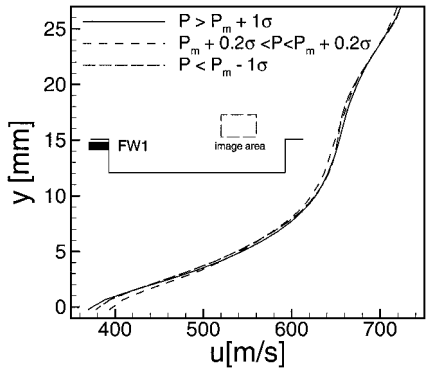

Fig. 18 Ensemble-average streamwise velocity profiles for station 4.

The next step was to separate out image pairs that corresponded to a certain front-wall pressure condition. This was done through a conditional analysis code, and image pairs were categorized for the high-pressure group:

$$P > \bar{P} + 1\sigma$$

the low-pressure group:

$$P < \bar{P} - 1\sigma$$

and the mean-pressure group:

$$\bar{P} - 0.2\sigma < P < \bar{P} + 0.2\sigma$$

where $\bar{P}$ is the mean pressure and σ is the standard deviation of the fluctuating-pressure signal. Out of 459 image pairs, the number of ensembles found for high-, low-, and mean-pressure groups were 68, 86, and 78, respectively. These image pairs were then used to obtain the ensemble-average vector field for each pressure group. The corresponding ensemble-average streamwise velocity U profiles are plotted in Fig. 18. The U profiles show no meaningful difference. This analysis was repeated with the same result for different pressure thresholds using 1.5σ and 2σ variations from the mean pressure value for high- and low-pressure groups.

The region from the front wall to 3.1 in. (7.9 cm) downstream was also imaged with three measuring stations, each of which covered a field of view of 1.1 in. (2.79 cm). The number of ensembles for these stations was about one-fifth of that of station 4. No meaningful variation was observed in the velocity profiles for the three different pressure groups.

Conclusions

Simultaneous planar laser imaging (PLS and PIV) and fluctuating-pressure measurements have been made for a rectangular cavity with L/H ratios of 6 and 7 under a Mach 5 turbulent shear layer. Analysis of previously acquired data under the same conditions for L/H ratios of 3, 4, and 5 has also been made. High-frequency response pressure transducers were installed in the top of the rear wall to monitor shear-layer impingement and in the front wall to examine a possible relation between the quasi-periodic pressure signal on the front wall and the shear-layer velocity profiles downstream. A fairly large number of PLS side-view single images and double-pulse image pairs have been acquired at different stations (i.e., rear wall, front wall, and midregion) of the cavity. The results suggest that the physics of this high-Mach-number cavity flow is quite different from that of lower speed flows:

1) Spectral analysis of the front-wall pressure signals shows that the front-wall pressure signal exhibits small-amplitude, but approximately periodic, pressure oscillations. Because the period for the pressure oscillations coincides with that of an acoustic wave traveling between the rear and the front walls, the source of these oscillations is believed to be acoustical. The resonance frequencies match the closed-box acoustic modes of the cavity.

2) Spectral and conditional analysis of the fluctuating-pressure signals on the rear wall show that the signal is dominated by shock impingement events that are not periodic. The duration of a shock impingement event is independent of L/H and is of the order of the time required for a large-scale shear-layer structure to convect past a given point.

3) The instantaneous PLS images show no evidence for coherent structures that are induced by the cavity acoustics. Analysis of the instantaneous PLS image pairs taken of the rear-wall region in conjunction with the rear-wall pressure signals shows that the impact of the large-scale shear-layer structures on the rear wall not only can change the duration of an existing shock but can also be the cause of the formation of the shock. These images also show that an expansion wave appears and disappears at the front wall, but it is not known if this is periodic or how it correlates with the quasi-periodic front-wall pressure signal.

4) Ensemble-average velocity profiles obtained from PIV vector fields at different locations of the shear layer do not yield any meaningful differences for different pressure conditions at the front wall.

Overall, it appears that the acoustical phenomena inside the cavity have little effect on the shear-layer dynamics, which suggests that there is little shear-layer/acoustics coupling in the current cavity flow. Furthermore, it is probably this lack of coupling that results in the presence of purely acoustic modes. For high-Mach-number cavity flows, the role of the shear layer simply may be to introduce broadband high-intensity noise into the cavity. Under this assumption, larger L/H results in higher-intensity acoustic oscillations because the shear layer impinges lower on the rear wall, thus introducing higher-energy noise into the cavity.

Acknowledgments

Support for this research has been provided through a grant from the Air Force Office of Scientific Research (F49620-97-1-0060) monitored by S. Walker. The particle image velocimetry instrumentation was acquired under Grant DAAG55-98-1-0062 by the Army Research Office, monitored by T. Doligalski. The authors gratefully acknowledge these sources of support.

References

[1]Charwat, A. F., Roos, J. N., Dewey, F. C., and Hitz, J. A., "An Investigation of Separated Flows-Part I: The Pressure Field," *Journal of the Aerospace Sciences*, Vol. 28, No. 6, 1961, pp. 457–470.

[2]Rockwell, D., and Naudascher, E., "Review—Self-Sustaining Oscillations of Flow Past Cavities," *Journal of Fluids Engineering*, Vol. 100, No. 2, 1978, pp. 152–165.

[3]Perng, S. W., "Passive Control of Pressure Oscillations in Hypersonic Cavity Flow," Ph.D. Dissertation, Dept. of Aerospace Engineering and Engineering Mechanics, Univ. of Texas, Austin, TX, Dec. 1996.

[4]Rossiter, J. E., "Wind-Tunnel Experiments on the Flow over Rectangular Cavities at Subsonic and Transonic Speeds," Aeronautical Research Council, Repts. and Memoranda 3438, London, Oct. 1964.

[5]Heller, H. H., and Bliss, D. B., "Physical Mechanism of Flow-Induced Pressure Fluctuations in Cavities and Concepts for Their Suppression," AIAA Paper 75-491, March 1975.

[6]Bauer, R. C., and Dix, R. E., "Engineering Model of Unsteady Flow in a Cavity," Calspan Corp./AEDC Operations, Arnold Engineering Development Center, TR-91-17, Tullahoma, TN, Dec. 1991.

[7]Sinha, N., Dash, S. M., Chidambaram, N., and Findlay, D., "Perspective on the Simulation of Cavity Aeroacoustics," AIAA Paper 98-0286, Jan. 1998.

[8]Leu, Y. L., and Dolling, D. S., "Passive Control of Pressure Oscillations in Cavity Flow with Store Release," *Proceedings of Royal Aeronautical Society Conference on "Wind Tunnel and Wind Tunnel Test Techniques,"* ISBN 1 85768 048 0, London, 1997, pp. 15.1–15.4.

[9]Perng, S. W., and Dolling, D. S., "Passive Control of Pressure Oscillations in Hypersonic Cavity Flow," AIAA Paper 96-0444, Jan. 1996.

[10]Ünalmis, Ö. H., Clemens, N. T., and Dolling, D. S., "Planar Laser Imaging of High-Speed Cavity Flow Dynamics," AIAA Paper 98-0776, Jan. 1998.

[11]Ünalmis, Ö. H., Clemens, N. T., and Dolling, D. S., "Planar Laser Imaging of a Supersonic Side-Facing Cavity," AIAA Paper 99-0297, Jan. 1999.

[12]Murray, R. C., and Elliott, G. S., "Compressible Shear Layer over a Two-Dimensional Cavity," AIAA Paper 98-0430, Jan. 1998.

[13]Beresh, S. J., "The Effects of the Incoming Turbulent Boundary Layer on a Shock-Induced Separated Flow Using Particle Image Velocimetry," Ph.D. Dissertation, Dept. of Aerospace Engineering and Engineering Mechanics, Univ. of Texas, Austin, TX, Aug. 1999.

[14]Rehm, J. E., "The Effects of Heat Release on Planar Jet Diffusion Flames," Ph.D. Dissertation, Dept. of Aerospace Engineering and Engineering Mechanics, Univ. of Texas, Austin, TX, May 1999.

[15]Franke, M. E., and Carr, D. L., "Effect of Geometry on Open Cavity Flow-Induced Pressure Oscillations," AIAA Paper 75-492, March 1975.

[16]Cattafesta, L. N., Garg, S., Kegerise, M. S., and Jones, G. S., "Experiments on Compressible Flow-Induced Cavity Oscillations," AIAA Paper 98-2912, June 1998.

[17]East, L. F., "Aerodynamically Induced Resonance in Rectangular Cavities," *Journal of Sound and Vibration*, Vol. 3, No. 3, 1966, pp. 277–287.

[18]Zhang, X., and Edwards, J. A., "An Investigation of Supersonic Oscillatory Cavity Flows Driven by Thick Shear Layers," *Aeronautical Journal*, Vol. 94, No. 940, 1990, pp. 355–364.

[19]Maciulaitis, A., "Improved Predication of Frequency Modes for Peak Amplitude Pressures in Simulated Bomb Bays at Mach 0.6 to 3.0," Grumman Aerospace Corp., Research Dept. Memorandum RM-708, Bethpage, NY, June 1980.

[20]Everest, F. A., *The Master Handbook of Acoustics*, 2nd ed., TAB Books/McGraw–Hill, Blue Ridge Summit, PA, 1989, pp. 87–88.

[21]Tam, C. K. W., and Block, P. J. W., "On the Tones and Pressure Oscillations Induced by Flow Over Rectangular Cavities," *Journal of Fluid Mechanics*, Vol. 89, Pt. 2, 1978, pp. 373–399.

[22]Krishnamurty, K., "Acoustic Radiation from Two-Dimensional Rectangular Cutouts in Aerodynamic Surfaces," NACA TN-3487, Aug. 1955.

[23]Heller, H. H., Holmes, D. G., and Covert, E. E., "Flow-Induced Pressure Oscillations in Shallow Cavities," *Journal of Sound and Vibration*, Vol. 18, No. 4, 1971, pp. 545–553.

[24]Clark, R. L., Kaufman, L. G., II, and Maciulaitis, A., "Aeroacoustic Measurements for Mach 0.6–3.0 Flows Past Rectangular Cavities," AIAA Paper 80-0036, Jan. 1980.

[25]Clemens, N. T., and Mungal, M. G., "Two- and Three-Dimensional Effects in the Supersonic Mixing Layer," *AIAA Journal*, Vol. 30, No. 4, 1992, pp. 973–981.

M. Samimy
Associate Editor